

RESEARCH ARTICLE

A novel small-scale self-focusing suppression method for post-compression in high peak power lasers

Shuren Pan^{1,2,†}, Fenxiang Wu^{1,†}, Yang Zhao¹, Jiabing Hu¹, Zongxin Zhang¹, Yi Xu^{1,4},
Yuxin Leng^{1,4}, Ruxin Li¹, and Efim Khazanov^{3,4}

¹State Key Laboratory of High Field Laser Physics and CAS Center for Excellence in Ultra-intense Laser Science, Shanghai Institute of Optics and Fine Mechanics (SIOM), Chinese Academy of Sciences, Shanghai, China

²Center of Materials Science and Optoelectronics Engineering, University of Chinese Academy of Sciences, Beijing, China

³Gaponov-Grekhov Institute of Applied Physics (IAP) of Russian Academy of Sciences, Moscow, Russia

⁴China–Russian Belt and Road Joint Laboratory on Laser Science, Shanghai Institute of Optics and Fine Mechanics, Chinese Academy of Sciences, Shanghai, China

(Received 27 November 2023; revised 25 March 2024; accepted 17 May 2024)

Abstract

A novel method, combining an asymmetric four-grating compressor (AFGC) with pulse post-compression, is numerically demonstrated to improve the spatial uniformity of laser beams and hence to suppress small-scale self-focusing (SSSF) during the beam propagation in nonlinear materials of high peak power lasers. The spatial uniformity of laser beams is an important factor in performing post-compression, due to the spatial intensity modulation, or hot spots will be aggravated during the nonlinear propagation and then seriously damage the subsequent optical components. Three-dimensional numerical simulations of post-compression are implemented based on a femtosecond laser with a standard compressor and an AFGC, respectively. The simulated results indicate that post-compression with the AFGC can efficiently suppress the SSSF and also shorten the laser pulses from 30 fs to sub-10 fs. This work can provide a promising route to overcome the challenge of SSSF and will be meaningful to promote the practical application of the post-compression technique in high peak power lasers.

Keywords: high peak power laser; post-compression; asymmetric four-grating compressor; small-scale self-focusing

1. Introduction

Thanks to the developments of the chirped pulse amplification (CPA) and optical parametric chirped pulse amplification (OPCPA)^[1,2] techniques, laser peak power has reached the 10 PW level, and the corresponding laser-focused peak intensity has reached 10^{22} W/cm² and even 10^{23} W/cm²^[3–6]. Such super-intense lasers can bring several significant breakthroughs and advances for high-field sciences^[7,8]. Nowadays, some countries have also commissioned the construction of 100 PW level ultrahigh peak power lasers^[9–12], to pursue higher laser intensity and hence to explore frontier sciences. As is well known, laser peak power can be enhanced by

increasing the pulse energy or by further shortening the pulse duration after the laser compressor. However, the limitation of peak power enhancement is no longer coming from pulse amplification, but rather from pulse compression, which is restricted by the available size and damage threshold of compression gratings. A multifold enhancement of peak power can only be implemented by using mosaic gratings in laser compressors or a coherent combination with several grating compressors. As a result, it entails a significant increase in the complexity, size and cost of ultrahigh peak power lasers. Shortening the pulse duration after the laser compressor, that is, post-compression, is obviously a promising approach to further enhance the peak power of lasers, which can be carried out without adding costly amplifiers and compression gratings. In addition, it is notable that the post-compression technique is also a potential way to develop compact and economical high peak power lasers.

The post-compression process generally consists of spectral broadening and pulse recompression^[12,13]. For

Correspondence to: Y. Xu and Y. Leng, State Key Laboratory of High Field Laser Physics and CAS Center for Excellence in Ultra-intense Laser Science, Shanghai Institute of Optics and Fine Mechanics (SIOM), Chinese Academy of Sciences, Shanghai 201800, China. Email: xuyi@siom.ac.cn (Y. Xu); lengyuxin@mail.siom.ac.cn (Y. Leng)

[†]These authors contributed equally to this work.

the post-compression of high peak power lasers, spectral broadening based on solid thin plates has been proved to be one of the suitable ways to shorten the pulse duration. As early as 2013, Voronin *et al.*^[14] proposed and simulated the generation of the subexawatt few-cycle pulses via the post-compression of a 13 PW/120 fs laser. In recent years, significant experimental progress has also been made in the post-compression of femtosecond lasers, with the peak power of hundreds of TW and even PW class^[15–18].

Although the pulse post-compression technique features undisputed merits, there are still some problems hindering its implementation, especially the small-scale self-focusing (SSSF) effect^[19]. It can result in significant impairment of beam quality, uncontrollable spectral broadening and the breakdown of optics. As is well known, the spatial intensity and phase modulation of high peak power lasers are usually relatively high, which is mainly induced by the defects of high-energy pump lasers and large-size gain media. Besides, hot spots will also appear due to diffraction on dust or due to optical defects. The spatial intensity modulation or hot spots will be further aggravated during the nonlinear propagation process, and then SSSF occurs and induces damage to the optics. Hence, SSSF suppression has become a key issue of the post-compression in high peak power lasers. On the one hand, SSSF can be suppressed by filtering the spatial perturbations during beam propagation in free space, that is, beam self-filtering with a specific spatial distance^[14–21]. On the other hand, the impacts of SSSF can be suppressed by improving the spatial uniformity of the laser beams before post-compression. To this end, spatial filters were employed before the laser compressor^[14,15]. However, spatial filters are high-cost and complex. Particularly for broadband high peak power lasers, for spatial filters it is necessary to consider not only the vacuum environment, but also their aberrations and possibly chromatic effects.

In this work, an asymmetric four-grating compressor (AFGC) is numerically demonstrated for suppressing SSSF during post-compression in high peak power lasers. The core aim of this method is to improve the spatial uniformity of the laser before post-compression by using an AFGC. It can provide a promising route to overcome the challenge of SSSF in traditional post-compression. Recently, a work about beam smoothing by introducing spatial dispersion was proposed for high peak power laser recompression^[22]. However, it

focused on the inhomogeneity of spectral broadening and peak power enhancement induced by the spatial nonuniformity of laser beams, and the effect on SSSF suppression has not been investigated or proved. Differently, this work mainly focuses on SSSF suppression by applying an AFGC. To clearly reveal the SSSF and demonstrate SSSF suppression by the AFGC, 3D simulations of post-compression with a higher resolution are carried out based on a femtosecond laser with a standard compressor and an AFGC, respectively. The numerical results show that post-compression after the AFGC can effectively suppress the SSSF and meanwhile shorten the pulses from 30 fs to sub-10 fs.

2. Post-compression after a standard compressor

Traditional post-compression for high peak power lasers with a standard compressor ($L_1 = L_2$) is shown in Figure 1. The compressed laser beam is firstly spectrally broadened through nonlinear transmission in thin plates (TTPs), and then dispersion compensated by chirped mirrors (CMs).

Assuming that the pulse spectrum (ranging from 750 to 850 nm) is 60 nm full width at half maximum (FWHM), the pulse duration is $\tau_{\text{FWHM}} = 30$ fs, the spatial beam fluence is a 10th super-Gaussian distribution and the spatial noise is a sinusoidal distribution for simplicity. Its corresponding maximal peak intensity in numerical simulations is about 2.8 TW/cm^2 . These parameters are set with reference to our SULF-1 PW laser beamline^[3], which is a typical femtosecond high peak power laser. The nonlinear media for spectral broadening are fused silica TTPs, with the group delay dispersion (GDD) of approximately $36 \text{ fs}^2/\text{mm}$ and a nonlinear refractive index of approximately $2.5 \times 10^{-7} \text{ cm}^2/\text{GW}$ at 800 nm central wavelength. The laser propagation in nonlinear media is simulated by a 3D nonlinear Schrödinger equation^[23], shown in Equation (1). Here, A is the envelope of electric field strength, z is the longitudinal coordinate, t is the time, β_2 is the group velocity dispersion, ω_0 and k_0 are the central frequency and central wavenumber, respectively, and n_0 and n_2 are the linear and nonlinear refractive index, respectively. As the gain spectra of modulation instability (also known as SSSF)^[24] generally features a cutoff around hundreds of mm^{-1} , which corresponds to transverse

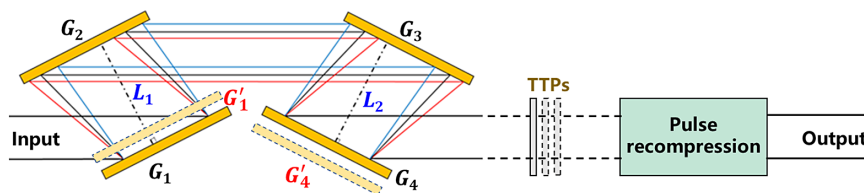


Figure 1. Setup of post-compression in high peak power lasers with a standard compressor (G_1 , G_2 , G_3 and G_4 , $L_1 = L_2$) and an AFGC (G'_1 , G_2 , G_3 and G_4 , $L_1 \neq L_2$).

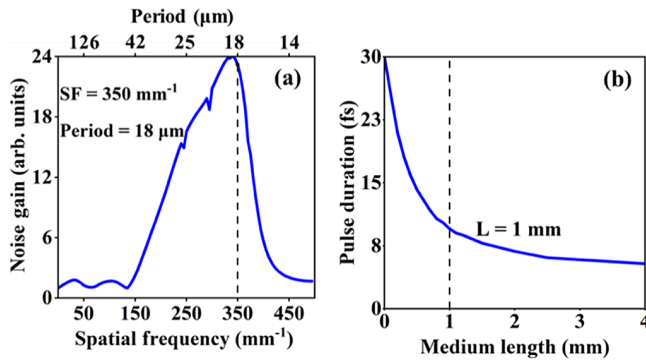


Figure 2. (a) The noise gain for different spatial frequency components. (b) The relationship between the achievable recompression pulse duration and the length of the fused silica TTPs.

uniformity of the beam profile with a typical size of a few micrometers, the resolution of our simulations is set as 2.5 μm. Besides, limited by computing power, a beam diameter of only 9 mm is adopted for numerical simulations and verifications. However, actually, the beam diameters of high peak power lasers are generally up to hundreds of millimeters:

$$\frac{\partial A}{\partial z} = \frac{i}{2k_0} \nabla_{\perp}^2 A + ik_0 \frac{n_2}{n_0} |A|^2 A - i \frac{\beta_2}{2} \frac{\partial^2 A}{\partial t^2} - k_0 \frac{n_2}{n_0 \omega_0} \frac{\partial (A \cdot |A|^2)}{\partial t}. \quad (1)$$

In the nonlinear propagation process, an arbitrary transverse wavevector K_{\perp} ($K_0 = 2\pi n_0 / \lambda_0$) propagates at an angle ($\theta = \pm K_{\perp} / K_0$) to the z -axis. In addition, the most serious characteristic angle is the direction in which the nonlinear process becomes phase matched, when considering the nonlinear contributions to the different characteristic angles. The most serious characteristic angle and corresponding spatial frequency can be calculated by Equation (2)^[12]:

$$\theta_{\max} = \sqrt{\frac{2n_2 I}{n_0}}; K_{\perp \max} = K_0 \theta_{\max} = \frac{2\pi n_0}{\lambda_0} \sqrt{\frac{2n_2 I}{n_0}}. \quad (2)$$

For the 30 fs laser assumed above, the noise gain for different spatial frequency components is calculated, as shown in Figure 2(a)^[25,26]. The noise gain is calculated as the ratio of the noise fluences after and before the spectral broadening process. For simplicity, the spatial frequencies of all noises in the laser are set to $K_{\perp \max}$ (the calculated result is $\sim 350 \text{ mm}^{-1}$) in the following spectral broadening process. On the one hand, the SSSF instability has the highest increment at this spatial frequency. Hence, if suppression at the peak of the instability gain, which shows the maximal SSSF suppression ability of this method, is satisfied, we may not need to be concerned about all the other ones. On the other hand, the noises at this frequency cannot be completely diffracted out by free propagation over a few meters in the compressors of ultrahigh peak power lasers, since their beam

diameters generally reach up to hundreds of millimeters. Beam cleaning in a standard compressor is not the point of this work; hence we neglected temporal self-filtering in standard compressors^[27].

To clearly show the physical nature of the AFGC in SSSF suppression, we used 30 fs pulses at each point of the beam cross-section and fluence distribution as a boundary condition for Equation (1) at $z = 0$. The attainable recompressed pulse durations of the 30 fs laser are also calculated based on the different lengths of the TTPs. As shown in Figure 2(b), sub-10 fs recompressed pulses can be achieved in the case of 1.0-mm-thick fused silica TTPs, which has also been experimentally proved in a similar femtosecond laser^[15]. Thereby, 1.0-mm-thick fused silica plates will be employed for spectral broadening in the following simulations, with a B-integral of approximately 5.5.

Figure 3(a) illustrates the spatial distribution of the initial 30 fs laser. The maximal beam fluence is 0.12 J/cm^2 and the PTA (peak-to-average) value of the beam fluence is 1.52. The left-hand and bottom curves correspond to the beam fluence on the central axis of the laser beam, and the same in the following figures. After passing through the 1.0-mm-thick fused silica TTPs, the fluence modulation becomes much more serious, and the maximal beam fluence greatly increases to 0.76 J/cm^2 , shown as Figure 3(b). Such a large beam fluence will seriously destroy the following optical components and prevent the practical application of post-compression. To reveal more detail, the small areas in Figures 3(a) and 3(b) are zoomed in, as shown in Figures 3(c) and 3(d). It is obvious that serious SSSF occurs during the above spectral broadening process. Hence, the suppression of SSSF should be a core issue in the post-compression of high peak power lasers.

3. Post-compression after an asymmetric four-grating compressor

The novel post-compression scheme based on AFGC^[28], that is, $L_1 \neq L_2$ in Figure 1, is proposed for high peak power lasers to overcome the challenge of SSSF. An AFGC can offer absolutely the same amount of temporal chirp for pulses compression as a standard compressor, as long as $L_2 + L_1$ are equal in both designs. Hence, the influence of residual temporal chirp on the following spectral broadening process can be ignored. By using the AFGC, a moderate spatial dispersion can be introduced to the output laser, which can effectively smooth the beam fluence^[28]. The AFGC-induced spatial dispersion length can be written as in Equation (3), where ω_s and ω_l represent the shortest and the longest wavelength components of the input laser, respectively, and α and β are the incident and diffracted angles on G_1 , respectively. It is obvious that the spatial dispersion length d_0 is proportional to the difference between L_1 and L_2 . Because of the relatively

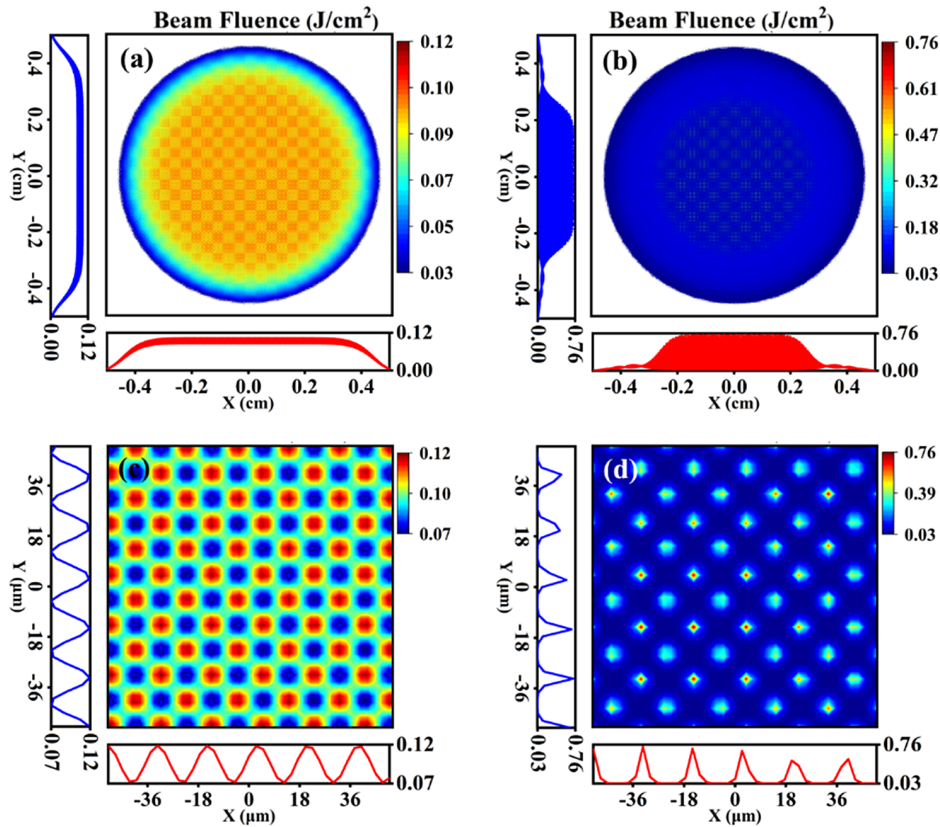


Figure 3. The spatial beam fluences of a 30 fs laser: (a) output from a standard compressor and (b) then after spectral broadening; (c), (d) zoomed-in of the corresponding areas in (a) and (b), respectively.

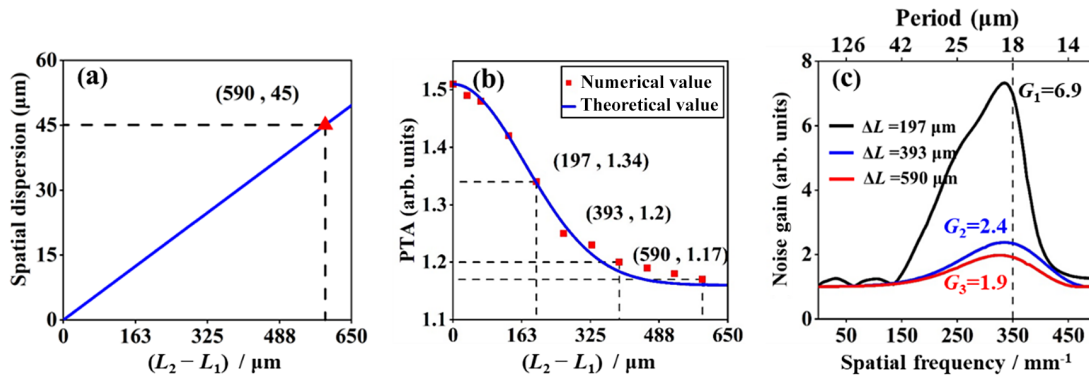


Figure 4. (a) The spatial dispersion and (b) the PTA of beam fluence output from the AFGC, based on different $L_2 - L_1$ of the AFGC. (c) The noise gain curves of laser beams after the AFGC with different $L_2 - L_1$.

strong diffraction ability of gratings, large spatial dispersion can be realized by a small $L_2 - L_1$:

$$d_0 = (\tan \beta(\omega_s) - \tan \beta(\omega_i)) \times \cos \alpha \times (L_2 - L_1). \quad (3)$$

In order to demonstrate the advantages of the AFGC in SSSF suppression, a numerical simulation is also carried out based on the same 30 fs laser parameters as above. For the standard compressor above, the grating groove density is 1480 gr/mm, the grating pair separations are 1.0 m and the laser incident angle on G_1 is $\alpha = 50^\circ$. These parameters

are also referring to the compressor in our SULF-1 PW laser beamline^[3]. To be an AFGC, two grating pair separations are altered, respectively, while keeping their sum constant (2 m). Figure 4(a) shows that the spatial dispersion length d_0 is proportional to the difference between L_1 and L_2 , while Figure 4(b) shows that the PTA drastically reduces with the increasing $L_2 - L_1$. The numerical simulation agrees well with the theoretical prediction (blue curve), which is deduced using Equations (8), (21), (27), (28) and (32) in Ref. [27]:

$$PTA_{\text{out}} = \exp\left(-\left(\frac{L_2 - L_1}{l}\right)^2\right) (PTA_{\text{in}} - PTA_{\text{ideal}}) + PTA_{\text{ideal}}, \quad (4)$$

where:

$$l = \frac{\omega_0 \tau_{\text{FWHM}}}{\sqrt{\ln 2} \cdot k_{\perp \text{max}}} \cdot \frac{\cos^3 \beta(\omega_0)}{(\sin \alpha + |\sin \beta(\omega_0)|) \cos \alpha}. \quad (5)$$

Here, $PTA_{\text{ideal}} = 1.16$ is the result of an ideal 10th super-Gaussian beam without noise, and ω_0 represents the central wavelength component of the input laser. The noise gain of the laser after the AFGC also reduces with the increase of $L_2 - L_1$, shown as Figure 4(c). In the case of $L_1 = 0.999705$ m, $L_2 = 1.000295$ m, the noise gain at 350 mm^{-1} dramatically drops to 1.9, while it is 24 when a standard compressor is adopted. This difference $L_2 - L_1 = 590 \text{ }\mu\text{m}$ is very small compared with the initial grating pair separation of 1 m. Hence, the slight influence on the spatiotemporal quality of compressed pulses can be ignored^[29]. Notably, the results in Refs. [27,28,30] have also proved that the temporal contrast and the focused peak intensity of compressed pulses output from an AFGC

remain almost unchanged, compared with that of a standard compressor.

The beam fluence output from the above AFGC is shown in Figure 5(a). It is clear that the fluence modulation is greatly decreased, and the maximal beam fluence is reduced from initial 0.12 to 0.09 J/cm^2 . Then, the smooth laser beam will also pass through the 1.0-mm-thick fused silica TTPs for spectral broadening. The output beam fluence is shown in Figure 5(b). As the noise gain is only 1.9, the maximal beam fluence is just increased to 0.09450 from 0.09446 J/cm^2 . In addition, there is no evident degradation of the fluence modulation or the spatial uniformity in the above spectral broadening process. The small areas that correspond to Figure 3 are also zoomed in and are shown in Figures 5(c) and 5(d). Before and after the TTPs, there is no obvious difference in beam quality. The simulation results prove that the SSSF is effectively suppressed by the AFGC. Compared with Figure 3(b), the SSSF-induced fluence modulation and intensity spikes are overcome and a more uniform laser beam is achieved.

For the sake of simplicity, the spectral broadening and recompressing of the above smooth laser beam are characterized by the simulated results based on the nonlinear

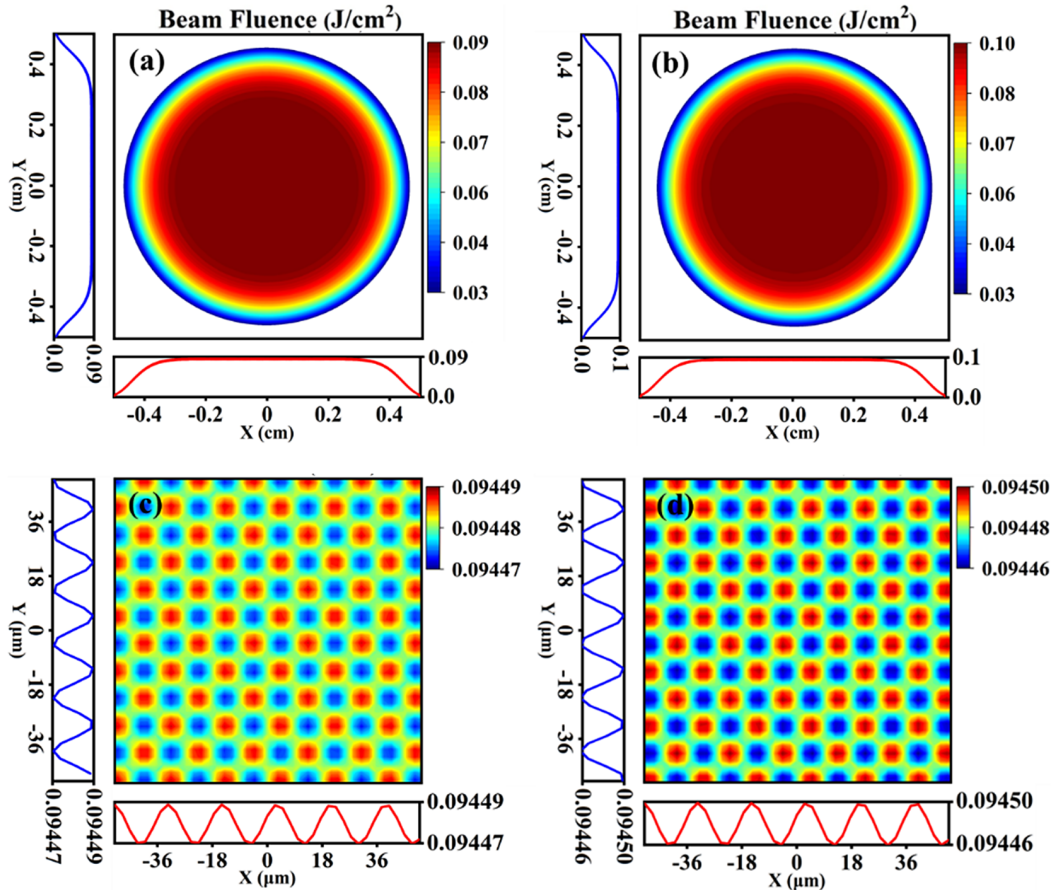


Figure 5. The spatial beam fluence of a 30 fs laser: (a) output from an AFGC and (b) then after the spectral broadening stage; (c), (d) zoomed-in of the corresponding areas in (a) and (b), respectively.

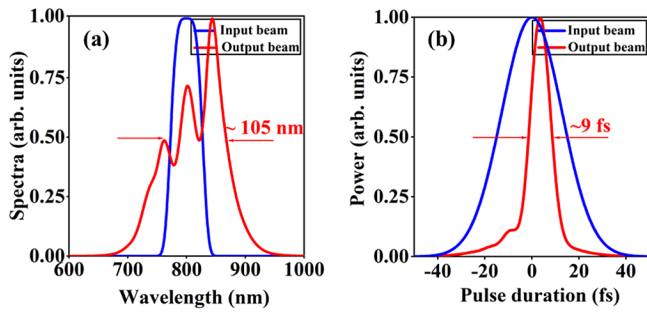


Figure 6. (a) The spectra of laser pulses before and after spectral broadening. (b) The pulse durations before and after post-compression with an AFGC.

Schrödinger equation, in which the laser intensity is approximated as the averaged intensity in the near-field. As a result, the spectral width is broadened from 60 nm to approximately 105 nm (FWHM), as shown in Figure 6(a). The asymmetry of the broadened spectrum is mainly induced by the self-steepening effect. Lastly, the residual dispersion of the spectral broadened laser is compensated by using broadband CMs. The additional GDD, introduced by the self-phase modulation (SPM) process and the nonlinear materials, is about 80 fs^2 . After being reflected by two broadband CMs with a total GDD of -80 fs^2 , sub-10 fs ultrashort laser pulses are expected, as shown in Figure 6(b).

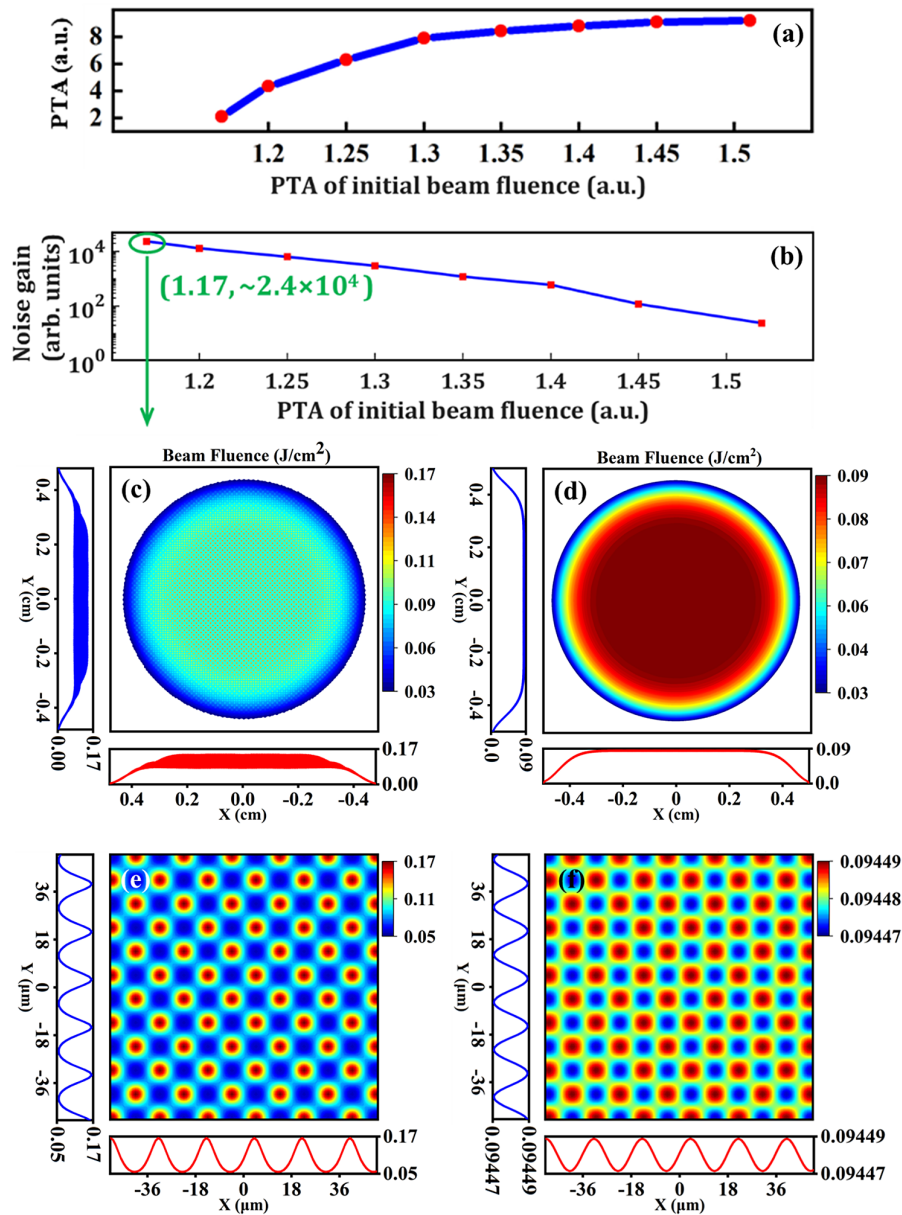


Figure 7. (a) The PTA of the beam fluence after spectral broadening with a 1-mm-thick TTP and (b) the corresponding noise gain, based on different initial laser beams. The beam fluences of lasers after spectral broadening with a 1-mm-thick TTP, with (c) a standard compressor and (d) an AFGC. (e), (f) Zoomed-in of the corresponding areas in (c) and (d), respectively.

4. Post-compression at different initial noise intensities

For the initial laser beams with different noise intensities compared to Figure 3(a), the PTAs of the beam fluence after the spectral broadening process and the corresponding noise gain are also investigated, as shown with the upper two curves in Figures 7(a) and 7(b). Due to the saturation effect, the PTA growth of output beam fluence gradually flattens out and the noise gain rapidly reduces, with the increase of initial noise fluence. Physically, the saturation can be explained by the reduction of fluence transferring from the main laser to the noise. When the noise fluence is high enough to be compatible with the main laser fluence, the instability increment decreases. In other words, the noise gain rapidly increases with the reduction of initial noise intensity, that is, the PTA of the initial beam fluence. The noise gain can reach approximately 2.4×10^4 when the initial PTA is 1.17. In this case, serious SSSF will occur in post-compression with a standard compressor, as shown in Figures 7(c) and 7(e), but a smooth laser beam still can be achieved by applying an AFGC ($L_2 - L_1 = 590 \mu\text{m}$, the same in all cases) before post-compression, as shown in Figures 7(d) and 7(f). Hence, an AFGC may be also indispensable for the post-compression of high peak power lasers, even if the laser beams before nonlinear media are good enough.

5. Conclusion

In summary, a novel method is numerically proved to suppress the SSSF for post-compression in high peak power lasers. The crucial point is the effective combination of an AFGC with post-compression, in which case the beam smoothing of the AFGC can be fully utilized for the following post-compression. The numerical results indicate that the AFGC can efficiently suppress the SSSF and meanwhile shorten the high peak power laser pulses from 30 to sub-10 fs. What is more, the AFGC is also indispensable for the post-compression of high peak power lasers, even if the beam quality of the lasers before nonlinear media is good enough. Hence, this method should be very meaningful to promote the practical application of post-compression in high peak power lasers.

Supplementary material

The supplementary material for this article can be found at <http://doi.org/10.1017/hpl.2024.31>.

Acknowledgements

This work was supported by the National Key R&D Program of China (2022YFE0204800, 2022YFA1604401, 2019YFF01014401); Shanghai Sailing Program

(21YF1453800); National Natural Science Foundation of China (11127901, 61925507); International Partnership Program of Chinese Academy of Sciences (181231KYSB20200040); Shanghai Science and Technology Committee Program (22560780100, 23560750200); Chinese Academy of Sciences President's International Fellowship Initiative (2023VMB0008); Ministry of Science and Higher Education of the Russian Federation (075-15-2020-906, Center of Excellence 'Center of Photonics'); and Youth Innovation Promotion Association of the Chinese Academy of Sciences.

References

1. M. D. Strickland and G. Mourou, *Opt. Commun.* **55**, 219 (1985).
2. A. Dubietis, G. Jonušauskas, A. Piskarskas, *Opt. Commun.* **88**, 437 (1992).
3. Z. Zhang, F. Wu, J. Hu, X. Yang, J. Gui, X. Liu, C. Wang, Y. Liu, X. Lu, Y. Xu, Y. Leng, R. Li, and Z. Xu, *High Power Laser Sci. Eng.* **8**, e4 (2020).
4. H. Kiriya, Y. Miyasaka, A. Kon, M. Nishiuchi, A. Sagisaka, H. Sasao, A. S. Pirozhkov, Y. Fukuda, K. Ogura, K. Kondo, N. P. Dover, and M. Kando, *High Power Laser Sci. Eng.* **9**, e62 (2021).
5. J. W. Yoon, Y. G. Kim, I. W. Choi, J. H. Sung, H. W. Lee, S. K. Lee, and C. H. Nam, *Optica* **8**, 630 (2021).
6. D. Umstadter, *Phys. Plasmas* **8**, 1774 (2001).
7. W. Wang, K. Feng, L. Ke, C. Yu, Y. Xu, R. Qi, Y. Chen, Z. Qin, Z. Zhang, M. Fang, J. Liu, K. Jiang, H. Wang, C. Wang, X. Yang, F. Wu, Y. Leng, J. Liu, R. Li, and Z. Xu, *Nature* **595**, 516 (2020).
8. J. Bromage, S.-W. Bahk, M. Bedzyk, I. A. Begishev, S. Bucht, C. Dorrer, C. Feng, C. Jeon, C. Mileham, R. G. Roides, K. Shaughnessy, M. J. Shoup III, M. Spilatro, B. Webb, D. Weiner, and J. D. Zuegel, *High Power Laser Sci. Eng.* **9**, e63 (2021).
9. E. Khazanov, A. Shaykin, I. Kostyukov, V. Ginzburg, I. Mukhin, I. Yakovlev, A. Soloviev, I. Kuznetsov, S. Mironov, A. Korzhimanov, D. Bulanov, I. Shaikin, A. Kochetkov, A. Kuzmin, M. Martyanov, V. Lozhkarev, M. Starodubtsev, A. Litvak, and A. Sergeev, *High Power Laser Sci. Eng.* **11**, 78 (2023).
10. E. Cartlidge, *Science* **355**, 785 (2017).
11. F. Wu, J. Hu, X. Liu, Z. Zhang, P. Bai, X. Wang, Y. Zhao, X. Yang, Y. Xu, C. Wang, Y. Leng, and R. Li, *High Power Laser Sci. Eng.* **10**, e38 (2022).
12. E. A. Khazanov, S. Y. Mironov, and G. Mourou, *Phys.-Uspekhi* **62**, 1096 (2019).
13. T. Nagy, P. Simon, and L. Veisz, *Adv. Phys. X* **6**, 1845795 (2020).
14. A. A. Voronin, A. M. Zheltikov, T. Ditmire, B. Rus, and G. Korn, *Opt. Commun.* **291**, 299 (2013).
15. J. I. Kim, Y. G. Kim, J. M. Yang, J. W. Yoon, J. H. Sung, S. K. Lee, and C. H. Nam, *Opt. Express* **30**, 8734 (2022).
16. V. Ginzburg, I. Yakovlev, A. Zuev, A. Korobeynikova, A. Kochetkov, A. Kuzmin, S. Mironov, A. Shaykin, I. Shaikin, E. Khazanov, G. Mourou, *Phys. Rev. A* **101**, 013829 (2020).
17. V. Ginzburg, I. Yakovlev, A. Kochetkov, A. Kuzmin, S. Mironov, I. Shaikin, A. Shaykin, and E. Khazanov, *Opt. Express* **29**, 28297 (2021).
18. A. Shaykin, V. Ginzburg, I. Yakovlev, A. Kochetkov, A. Kuzmin, S. Mironov, I. Shaikin, S. Stukachev, V. Lozhkarev,

- A. Prokhorov, and E. Khazanov, *High Power Laser Sci. Eng.* **9**, e54 (2021).
19. S. Mironov, V. Lozhkarev, G. Luchinin, A. Shaykin, and E. Khazanov, *Appl. Phys. B* **113**, 147 (2013).
20. M. Martyanov, V. Ginzburg, A. Balakin, S. Skobelev, D. Silin, A. Kochetkov, I. Yakovlev, A. Kuzmin, S. Mironov, I. Shaikin, S. Stukachev, A. Shaykin, E. Khazanov, and A. Litvak, *High Power Laser Sci. Eng.* **11**, e28 (2023).
21. V. N. Ginzburg, I. V. Yakovlev, A. S. Zuev, A. P. Korobeynikova, A. A. Kochetkov, A. A. Kuz'min, S. Y. Mironov, A. A. Shaykin, I. A. Shaikin, and E. A. Khazanov, *Quantum Electron.* **49**, 29 (2019).
22. H. Xi, X. Tang, Y. Liu, J. Bin, and Y. Leng, *Opt. Express* **31**, 33754 (2023).
23. H. Zia, *Commun. Nonlinear Sci. Numer. Simulat.* **54**, 356 (2018).
24. V. I. Bespalov and V. I. Talanov, *JETP* **3**, 307 (1966).
25. E. S. Bliss, J. T. Hunt, P. A. Renard, G. E. Sommargwn, and H. J. Weaver, *Quantum Electron.* **12**, 402 (1976).
26. V. N. Ginzburg, A. A. Kochetkov, A. K. Potemkin, and E. A. Khazanov, *Quantum Electron.* **48**, 325 (2018).
27. E. Khazanov, *High Power Laser Sci. Eng.* **11**, e93 (2023).
28. X. Shen, S. Du, W. Liang, P. Wang, J. Liu, and R. Li, *Appl. Phys. B* **128**, 159 (2022).
29. C. Wang, D. Wang, Y. Xu, and Y. Leng, *Opt. Commun.* **507**, 127613 (2022).
30. S. Du, X. Shen, W. Liang, P. Wang, J. Liu, and R. Li, *High Power Laser Sci. Eng.* **11**, e4 (2023).